

# Analytical Derivation of Electrical-Side Maximum Power Line for Wind Generators

Sergei Kolesnik<sup>1</sup> and Alon Kuperman<sup>1,2,\*</sup> 

<sup>1</sup> Department of Electrical Engineering and Electronics, Ariel University of Samaria, Ariel 40700, Israel; skolesnik@gmail.com

<sup>2</sup> Department of Electrical and Computer Engineering, Ben-Gurion University of the Negev, Beer-Sheva 84105, Israel

\* Correspondence: alonk@bgu.ac.il; Tel.: +972-526-943-234

Academic Editor: Marco Mussetta

Received: 16 August 2017; Accepted: 25 September 2017; Published: 26 September 2017

**Abstract:** In order to enhance the maximum power point tracking (MPPT) speed of solar generators, offline calculated maximum power line (MPL) is often used as a feed-forward signal added to the output of MPPT controller. MPL is nonlinear static electrical characteristic of renewable energy generators connecting all the maximum power points for given temperature. In this letter, electrical side MPL is derived for a typical wind turbine generator (WTG). It is shown that MPLs of solar and wind generators possess similar structure, supporting the similarity between the two energy conversion processes.

**Keywords:** wind turbine generator; MPPT; maximum power line

## 1. Introduction

Renewable energy sources possess the so-called *soft source* characteristics, requiring careful interfacing (i.e., maximum power point tracking, MPPT) to allow optimal utilization in terms of cost and reliability [1,2]. A generalized renewable energy conversion system is shown in Figure 1, consisting of a renewable energy generator (REG), an interfacing power converter (IPC), and a load.

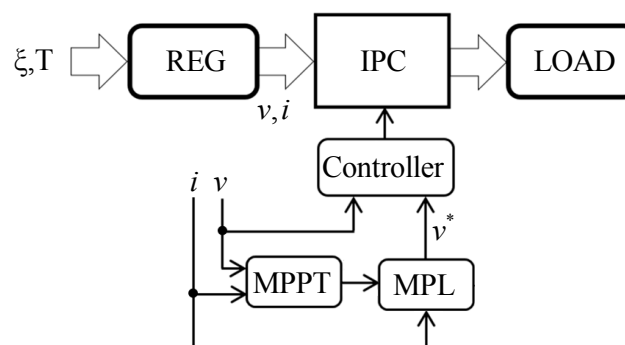


**Figure 1.** Generalized renewable energy conversion system operating in maximum power point tracking (MPPT) mode. IPC: interfacing power converter; MPL: maximum power line; REG: renewable energy generator.

Typical inputs affecting REG operation are the energy producing variable  $\xi$  (solar irradiation, wind, etc.) and the temperature  $T$ . On the electrical side of the REG, voltage and current are sampled and fed back into an MPPT algorithm in order to utilize as much harvested energy as possible [3,4].

In order to increase the response time of conventional (MPP) trackers and decrease the effect of fast varying energy processing variable, the authors of [5] proposed the inclusion of a feed-forward term which predicts REG MPP voltage ( $v^*$ ) from measured REG current  $I$  according to a priori calculated MPL, as shown in Figure 2. Thus, the feed-forward term brings the operational point of the IPC to the vicinity of MPP and the tracker performs only the fine-tuning required due to parameter inaccuracies and slow varying temperature. The method is used in both solar [6] and wind [7] energy conversion systems; nevertheless, the latter typically employ mechanical rather than electrical side MPL, utilizing torque control requiring mechanical sensors [8]. In this brief, electrical side MPL is derived for wind generators, treated as electrical sources to allow application of the well-studied methods of interfacing photovoltaic generators to wind turbine generators without the need of mechanical sensors.

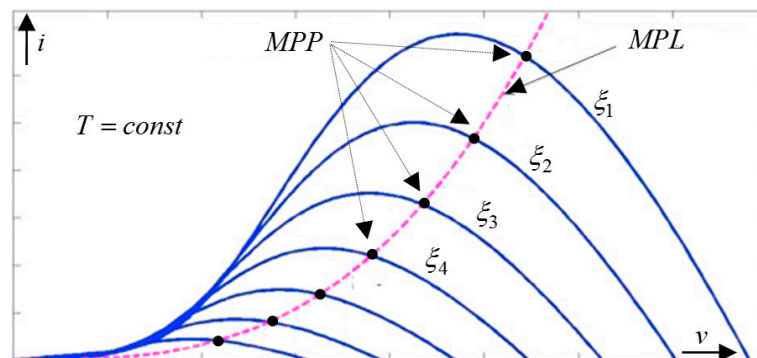


**Figure 2.** Electrical side REG characteristics for different values of energy producing variable and corresponding MPL.

## 2. Wind Turbine Generator (WTG) MPL Derivation

Wind power extracted by a wind turbine is given by [9]

$$P_W = \frac{1}{2} \rho A C_P v_W^3, \tag{1}$$

where  $\rho$  is air density,  $A$  is the area swept by turbine's blades,  $v_W$  is wind speed, and  $C_P$  is power coefficient, which is a nonlinear function of turbine tip-speed ratio ( $TSR$ ), given by

$$TSR = \frac{\omega_T R}{v_W}, \tag{2}$$

with  $R$  denoting blade radius. Substituting (3) into (2), there is

$$P_W = \frac{1}{2} \rho A C_P \left( \frac{R}{TSR} \right)^3 \omega_T^3. \tag{3}$$

The typical  $C_P$ -versus- $TSR$  curve is bell-shaped, possessing a single MPP, defined by  $(TSR_{OPT}, C_{P,MAX})$  pair which is constant for a given wind turbine. Hence, maximum power is extracted from the wind blowing with speed  $v_W$  by rotating the turbine at

$$\omega_{T,MPP} = \frac{TSR_{MPP}}{R} v_W \tag{4}$$

and is given by

$$P_{W,MPP} = \underbrace{\frac{1}{2} \rho A C_{P,MAX} \left( \frac{R}{TSR_{OPT}} \right)^3}_{K_{MPP}} \omega_{T,MPP}^3 = K_{MPP} \omega_{T,MPP}^3. \tag{5}$$

Note that  $K_{MPP}$  is temperature-dependent since it is influenced by air density. Consequently, the relation between wind-produced torque and turbine speed at MPP is given by

$$T_{W,MPP} = \frac{P_{W,MPP}}{\omega_{T,MPP}} = K_{MPP}\omega_{T,MPP}^2 \Leftrightarrow \omega_{T,MPP} = \sqrt{K_{MPP}^{-1}T_{W,MPP}}, \quad (6)$$

defining mechanical MPL of the wind turbine, typically used in the literature.

Consider (without loss of generality) a WTG, consisting of wind turbine WT, driving DC generator (DCG) via stiff gear  $G$ , as shown in Figure 3. Low-frequency dynamics of the WTG is governed by

$$J_T\dot{\omega}_T + B_T\omega_T = T_W - T_T = \frac{P_W}{\omega_T} - T_T, \quad (7)$$

where  $J_T$  and  $B_T$  are turbine moment of inertia and friction coefficient, respectively,  $\omega_T$  is turbine angular speed,  $T_W$  is wind-produced torque, and  $T_T$  is DCG torque, reflected to the low-speed turbine shaft. The transmission relates turbine and generator speeds and torques as

$$G = \frac{\omega_M}{\omega_T} = \frac{\eta_G T_T}{T_M} \quad (8)$$

with  $\eta_G$  denoting gear efficiency. Dynamics of the generator mechanical part is governed by

$$J_M\dot{\omega}_M + B_M\omega_M = T_M - \frac{K_T i}{\eta_M}, \quad (9)$$

where  $J_M$ ,  $B_M$ , and  $\eta_M$  are machine moment of inertia, friction coefficient, and efficiency, respectively,  $i$  is DCG output current, and  $K_T$  is DCG torque constant. Combining (7)–(9), generator-side dynamics is obtained as

$$J_M^{EQ} \frac{d\omega_M}{dt} + B_M^{EQ} \omega_M = \frac{\eta_G}{G} T_W - \frac{K_T i}{\eta_M} \quad (10)$$

with

$$J_M^{EQ} = J_M + \frac{J_T \eta_G}{G^2}, \quad B_M^{EQ} = B_M + \frac{B_T \eta_G}{G^2}. \quad (11)$$

Electrical side DCG behavior is described by

$$L_M \dot{i} + R_M i = e - v = K_T \omega_M - v \quad (12)$$

with  $L_M$  and  $R_M$  denoting machine coil inductance and resistance, respectively,  $e = K_T \cdot \omega_M$  signifying back electromotive force and  $v$  symbolizing DCG terminal voltage. Since electrical time constant is typically much lower than the mechanical one, (12) may be approximated by

$$v \cong e - R_M i, \quad (13)$$

neglecting phase inductance dynamics. Further substituting DCG speed with back electromotive force results in the electrical-side system of equations, given by

$$\begin{cases} \frac{J_M^{EQ}}{K_T} \frac{de}{dt} + \frac{B_M^{EQ}}{K_T} e = \frac{\eta_G}{G} T_W - \frac{K_T i}{\eta_M} \\ v = e - R_M i \end{cases} \quad (14)$$

In steady state, (14) reduces to

$$\begin{cases} \frac{B_M^{EQ} \eta_M}{K_T^2} e = \frac{\eta_G \eta_M}{G K_T} T_W - i \\ v = e - R_M i \end{cases} \quad (15)$$

Combining (6) and (8) with (15) gives after rearranging

$$\begin{cases} e^2 - \frac{B_M^{EQ} K_T G^3}{\eta_G K_{MPP}} e - \frac{K_T^3 G^3}{\eta_M \eta_G K_{MPP}} i = 0 \\ v = e - R_M i \end{cases} \quad (16)$$

Electrical-side MPL is obtained by solving (16) as

$$v = \frac{B_M^{EQ} K_T G^3}{2\eta_G K_{MPP}} + \sqrt{\left(\frac{B_M^{EQ} K_T G^3}{2\eta_G K_{MPP}}\right)^2 + \frac{K_T^3 G^3}{\eta_M \eta_G K_{MPP}} i} - R_M i. \quad (17)$$

In some cases, REG power rather than voltage is fed back to the controller; i.e., power-voltage plane MPL is required, obtained as

$$p = \frac{B_M^{EQ} K_T G^3}{2\eta_G K_{MPP}} i + \sqrt{\left(\frac{B_M^{EQ} K_T G^3}{2\eta_G K_{MPP}} i\right)^2 + \frac{K_T^3 G^3}{\eta_M \eta_G K_{MPP}} i^3} - R_M i^2. \quad (18)$$

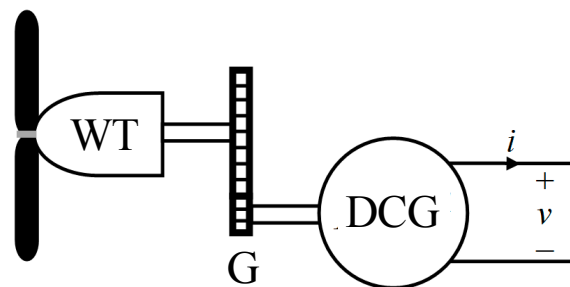
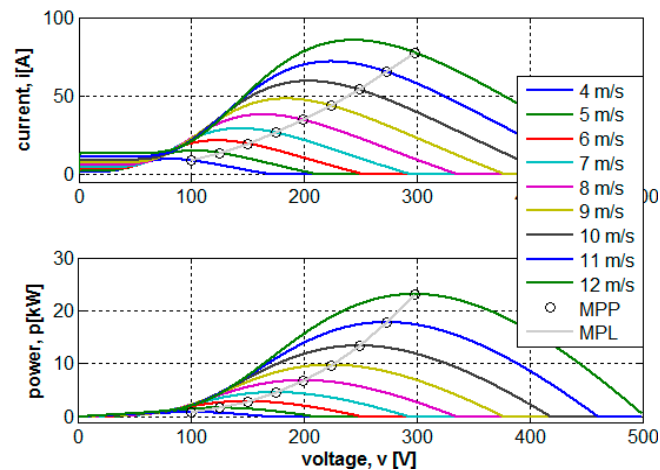


Figure 3. Wind turbine generator under study.

### 3. Numerical Example

Consider a WTG-DCG system, shown in Figure 3, characterized by the following parameters:

Turbine nominal power 24 kW, base wind speed 12 m/s, base rotational speed 60 rpm, total moment of inertia  $10 \times 10^{-3} \text{ N}\cdot\text{m}\cdot\text{s}^2/\text{rad}$ ,  $K_T = 0.02 \text{ Nm/A}$ , gear ratio 10, DCG rotor resistance  $40 \text{ m}\Omega$ . Power coefficient versus tip-speed ratio was adopted from [10]. Figure 4 presents the electrical side characteristics of the system for different wind speeds at  $25^\circ\text{C}$  with corresponding MPPs specified by circles. The MPLs shown were calculated according to (17) and (18). It may be concluded that estimated MPLs accurately link all the indicated MPPs in both current and power domains.



**Figure 4.** Electrical side characteristics of the wind turbine generator (WTG)-DC generator (DCG) and MPLs calculated according to (17) and (18).

#### 4. Discussion

Several important remarks should be emphasized as follows:

1. Even though a simple model of a DC Generator was utilized, it may be easily shown that in case permanent magnet generator (PMG) driving a three-phase diode rectifier (DR) is utilized, the solution form remains (some scaling should be carried out). Interested readers are referred to [7,11] for detailed modeling of a PMG-DR unit.
2. The derived expression (17) contains  $K_{MPP}$  and is therefore temperature-dependent. This is the main reason (apart from parameter uncertainty and possible variations) for the necessity of employing MPPT algorithm in addition to utilizing MPL. Nevertheless, since both temperature and parameter variations are relatively slow, high-bandwidth MPPT is unnecessary.
3. The MPL for solar generators was recently derived in [12] and is given by

$$v = \chi(T, i) - R_s i, \quad (19)$$

where  $\chi(\cdot)$  is a nonlinear operator (Lambert-W function related) and  $R_s$  is solar generator output series resistance. Note that the form of (18) is similar to that of (17), including temperature dependence. This further supports the similarity between solar and wind generators, recently pointed out in [13].

4. It should be pointed out that if friction and series resistance are neglected, (17) reduces to

$$v = \sqrt{\frac{K_T^3 G^3}{\eta_M \eta_G K_{MPP}}} i, \quad (20)$$

indicating pure quadratic relation between DC current and voltage. This result was reported in some earlier works. Furthermore, comparing (19) to the right-hand side of (6) reveals that in case the DCG is lossless (i.e., perceived as an ideal mechanical-to-electrical energy transformer), (19) is a mechanical-to-electrical domain transformation of (6); i.e.,  $v \sim \omega_T$  and  $i \sim T_W$ .

#### 5. Conclusions

In this brief, electrical-side MPL for wind turbine generators was derived. The finding allows a wind generator to be treated as an electrical source and thus potentially makes it possible to apply well-studied methods of interfacing photovoltaic generators to wind turbine generators.

Moreover, mechanical sensorless operation is enabled, requiring information regarding electrical-side variables only.

**Conflicts of Interest:** The authors declare no conflict of interest.

## References

1. Gadelovits, S.; Kuperman, A.; Sitbon, M.; Aharon, I.; Singer, S. Interfacing renewable energy sources for maximum power transfer—Part I: Statics. *Renew. Sustain. Energy Rev.* **2014**, *31*, 501–508. [[CrossRef](#)]
2. Kolesnik, S.; Sitbon, M.; Gadelovits, S.; Suntio, T.; Kuperman, A. Interfacing renewable energy sources for maximum power transfer—Part II: Dynamics. *Renew. Sustain. Energy Rev.* **2015**, *51*, 1771–1783. [[CrossRef](#)]
3. Kumar, D.; Chatterjee, K. A review of conventional and advanced MPPT algorithms for wind energy systems. *Renew. Sustain. Energy Rev.* **2016**, *55*, 957–970. [[CrossRef](#)]
4. Kolesnik, S.; Kuperman, A. On the equivalence of major variable-step size MPPT algorithms. *IEEE J. Photovolt.* **2016**, *6*, 590–594. [[CrossRef](#)]
5. Sokolov, M.; Shmilovitz, D. A modified MPPT scheme for accelerated convergence. *IEEE Trans. Energy Convers.* **2008**, *23*, 1105–1107. [[CrossRef](#)]
6. Scarpa, V.; Buso, S.; Spiazzi, G. Low-complexity MPPT technique exploiting the PV module MPP locus characterization. *IEEE Trans. Ind. Electron.* **2009**, *56*, 1531–1538. [[CrossRef](#)]
7. Xia, Y.; Ahmed, K.; Williams, B. Wind turbine power coefficient analysis of a new maximum power point tracking technique. *IEEE Trans. Ind. Electron.* **2013**, *60*, 1122–1132. [[CrossRef](#)]
8. Tan, K.; Islam, S. Optimum control strategies in energy conversion of PMSG wind turbine system without mechanical sensors. *IEEE Trans. Energy Convers.* **2004**, *19*, 392–399. [[CrossRef](#)]
9. Duong, M.Q.; Grimaccia, F.; Leva, S.; Musetta, M.; Le, K.H. Improving transient stability in a grid-connected squirrel-cage induction generator wind turbine system using a fuzzy logic controller. *Energies* **2015**, *8*, 6328–6349. [[CrossRef](#)]
10. Heier, S.; Waddington, R. *Grid Integration of Wind Energy Conversion Systems*; Wiley: Chichester, UK, 2006.
11. Dalala, Z.; Zahid, Z.; Lai, J. New overall control strategy for small scale WECS in MPPT and stall regions with mode transfer control. *IEEE Trans. Energy Convers.* **2013**, *28*, 1082–1092. [[CrossRef](#)]
12. Kolesnik, S.; Sitbon, M.; Lineykin, S.; Batzelis, E.; Papathanassiou, S.; Suntio, T.; Kuperman, A. Solar irradiation independent expression for photovoltaic generator maximum power line. *IEEE J. Photovolt.* **2017**, *7*, 1416–1420. [[CrossRef](#)]
13. Kolesnik, S.; Kuperman, A. On the similarity between low-frequency equivalent circuits of photovoltaic and wind generators. *IEEE Trans. Energy Convers.* **2015**, *30*, 407–409. [[CrossRef](#)]



© 2017 by the authors. Licensee MDPI, Basel, Switzerland. This article is an open access article distributed under the terms and conditions of the Creative Commons Attribution (CC BY) license (<http://creativecommons.org/licenses/by/4.0/>).